Molecular beam epitaxy and microstructural study of $La_{2-x}Sr_{1+x}Cu_2O_{6+y}$ thin films

K. Verbist, O. Milat, and G. Van Tendeloo
EMAT, RUCA, University of Antwerp, Groenenborgerlaan 171, B-2020 Antwerp, Belgium

F. Arrouy,* E. J. Williams, C. Rossel, E. Mächler, and J.-P. Locquet
IBM Research Division, Zurich Research Laboratory, CH-8803 Rüschlikon, Switzerland

(Received 27 November 1996)

Thin films of $La_2SrCu_2O_{6+y}$ with varying Sr/La ratios have been grown by molecular beam epitaxy on (001) $SrTiO_3$; their structural as well as their transport properties are reported. Under appropriate conditions, thin films with a metal-like resistivity down to 8 K are obtained; i.e., these films are closer to the onset of superconductivity than previous results indicate for bulk samples. This observation might be explained by a thin-film-specific alteration in site occupation of the La and Sr atoms in the lattice. In addition, the defect structures of a typical sample have been studied by transmission electron microscopy and the thin-film/substrate interface structure is determined. Out-of-phase boundaries with displacement vectors $R=[00\frac{1}{5}]$ occur throughout the entire film thickness. Such interfaces, which possibly originate at substrate surface steps, disconnect the CuO_2 layers and negatively influence eventual superconductivity. The films contain copper oxide outgrowths and nano-sized *a*-axis grains at the surface. Locally a $2\sqrt{2}a_p\times 2\sqrt{2}a_p$ modulation is observed; we have determined its unit cell and compared it with other so-called $2\sqrt{2}a_p\times 2\sqrt{2}a_p$ structures occurring in other superconducting compounds such as $YBa_2Cu_3O_{7-d}$ and $Bi_{1.8}Pb_{0.4}Sr_2Ca_2Cu_3O_{10+x}$. [S0163-1829(97)01426-4]

I. INTRODUCTION

The material $La_2SrCu_2O_{6+y}$ can be classified as belonging to the generic class 0212 and is the $n=2$ member of the Ruddlesden-Popper-type series $A_{n+1}B_nO_{3n+1}$ of which the well-known $La_{2-x}Sr_xCuO_4$ is the $n=1$ member. The pure $La_2SrCu_2O_{6+y}$ compound (containing only Sr) has never been made superconducting,[1–3] although a Ca-doped 0212 compound, $La_{1.6}Sr_{0.4}CaCu_2O_{6+y}$, has been found to superconduct with a $T_c=60$ K (Cava *et al.*[4]). Subsequently, 0212 compounds with various mixtures of La, Ca, Sr, and Ba as their *A* element were rendered superconducting either by using high-pressure oxygen annealing or by synthesis routes involving heating in the presence of $KClO_3$.

The room-temperature basic structure of $La_2SrCu_2O_{6+y}$ (Refs. 5,6) is body-centered tetragonal with space group $I4/mmm$ and lattice constants $a_p=b_p=0.386$ nm, $c\simeq 2.0$ nm (Fig. 1). The unit cell comprises two 0.99-nm-thick unit slabs with the stacking sequence (La,Sr)O-CuO_2-(La,Sr)-CuO_2-(La,Sr)O and a shift of $\frac{1}{2}[110]p$ between them. The distribution of La and Sr, however, is not completely statistical. The single fluorite-type (*F*-type) layer (with low oxygen fraction) between the CuO_2 sheets is predominantly occupied by La ($\simeq 80\%$), whereas the distribution of La and Sr in the double rocksalt-type (RS-type) layer approaches 60% and 40%, respectively.[7,8]

We have grown a series of *c*-axis $La_2SrCu_2O_{6+y}$ thin films on (001) $SrTiO_3$ (STO) with varying Sr/La ratios, i.e., a deposited stoichiometry which varies approximately from $La_{1.8}Sr_{1.2}Cu_2O_{6+y}$ to $La_{2.17}Sr_{0.83}Cu_2O_{6+y}$, and discuss here the temperature-composition phase diagram relevant to the growth conditions, as well as the variation of the structural and normal-state transport properties. In addition, we report on transmission electron microscopy (TEM) observations of the local structure and defects in one of these films (of composition $La_{1.8}Sr_{1.2}Cu_2O_{6+y}$), and present a local $2\sqrt{2}a_p\times 2\sqrt{2}a_p$ modulation found in some of the $La_2SrCu_2O_{6+y}$ thin films, discussing the structural modifications which may be at the origin of such a modulation.

II. EXPERIMENT

$La_2SrCu_2O_{6+y}$ thin films were grown by molecular beam epitaxy (MBE), and the installation is equipped with four effusion cells (one for strontium), two electron beam

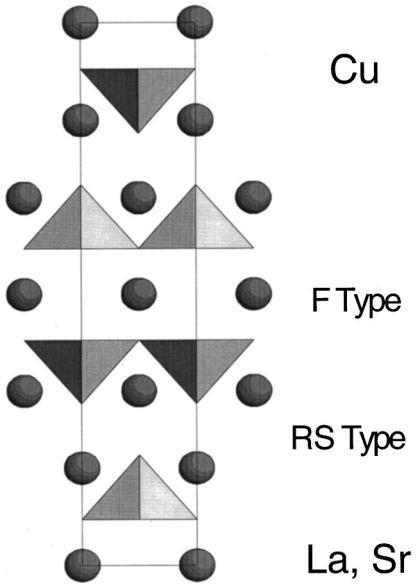

FIG. 1. Structure of the 0212 compound.

evaporators (copper and lanthanum), two quartz monitors, a quadrupole mass spectrometer, a rf plasma source,[9] and a reflection high-energy electron-diffraction (RHEED) system. The base pressure of the (unbaked) system is about 10^{-9} mbar, whereas during growth an oxygen background pressure of approximately 2×10^{-6} mbar was applied. A sequential deposition process was used, whereby the molecular beam flux is controlled by the mass spectrometer, which is previously calibrated using quartz monitors.

The films were deposited onto $SrTiO_3$ substrates heated to between 660 and 720 °C at an evaporation rate of three to six monolayers per minute using the following deposition sequence for each unit cell: two monolayers of La, one monolayer of Sr, and two monolayers of Cu. This is followed by a 10-s anneal under a continuous flow of atomic oxygen. A more detailed account of this block-by-block deposition method can be found in Ref. 10. The typical film thicknesses were around 40 nm. During the ''cool-down'' step, the heater power is turned off completely, and cooling takes place for more than 2 h under the same flow of atomic oxygen until the pyrometer reads below 100 °C.

The nominal composition of the thin films is within approximately ±10% of the values measured with the quartz monitors. A more precise estimate was obtained for two samples using Rutherford backscattering (RBS). The surface of the samples was imaged with an atomic force microscope (AFM) (Digital Instruments Nanoscope II). The probe was a microfabricated Si tip with a spring constant of 50 N/m. The image was processed using only a plane fit without low-pass filtering. The structural properties of the as-grown thin films were analyzed using a θ-2θ Siemens D500 x-ray-diffraction (XRD) system.

To study the oxidation behavior of the films, electrochemical experiments were performed at 300 K, at ambient, in a 1-mol KOH-solution-filled cell equipped with three electrodes: (i) The reference electrode: Hg/HgO filled with 1 mol KOH [$E_{th}=0.098$ V/SHE (standard hydrogen electrode)]. All potentials quoted in this work refer to this electrode. (ii) The counterelectrode: a large-area platinum foil. (iii) The working electrode: the thin film fully immersed in the electrolyte except for the upper part, which is contacted with the electrical circuit via a mechanical clamp. The geometrical surface area (S_g) in contact with the solution is $\simeq0.8$ cm^2.

The transport properties were measured by pressing four indium strips onto the film surface and creating a four-point contact. TEM observations were made using both plan-view (PV) and cross-section (CS) samples, which were prepared from the thin films by polishing with diamond paste or by polishing on diamond lapping foils with water as the lubricant, followed by ion milling until perforation. No difference was observed between samples prepared with or without water as the lubricant. High-resolution electron-microscopy (HREM) and electron-diffraction (ED) investigations were performed with a JEOL 4000 EX and a Philips CM 20 microscope. Image simulations of the HREM results were carried out using the Mac Tempas software.

III. RESULTS

A. Phase diagram

Besides the $La_2SrCu_2O_{6+y}$ phase, other ternary oxides exist in the La-Sr-Cu-O phase diagram, such as $La_{8-x}Sr_xCu_8O_{20}$ (808),[11] $La_2Sr_6Cu_8O_{16+\delta}$,[12] $La_{6.16}Sr_{1.84}Cu_{7.66}O_{20}$,[13] and $La_{2-x}Sr_xCuO_4$ (214). For our films, the only other ternary oxide that appeared in the XRD spectra was the 214 phase. As the films are grown at a constant ''atomic'' oxygen pressure, the appearance of this phase is controlled primarily by the composition and the substrate temperature.

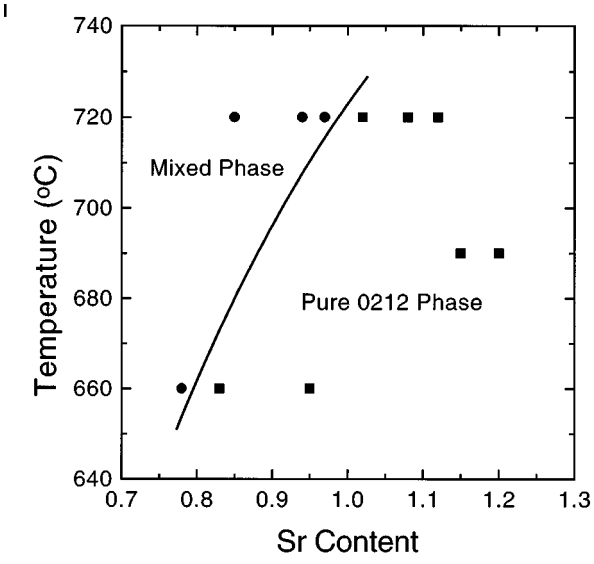

FIG. 2. Temperature-composition phase diagram at constant oxygen background pressure.

Figure 2 shows a temperature-composition phase diagram, indicating that the phase boundary of the pure Sr-doped ''0212'' phase shifts with increasing temperature to higher Sr values for a constant atomic oxygen pressure. At higher temperatures it becomes increasingly difficult to substitute large numbers of Sr atoms by La atoms in the 0212 lattice. Consequently the *F*-type layer between the two CuO_2 sheets disappears as the 214 structure forms.

B. Structural properties

1. X-ray diffraction

The XRD spectra from the thin films reveal a *c*-axis growth with very small impurity peaks, mainly CuO and 214. Samples with impurity peaks larger than 0.01% of those from the 0212 *c*-axis material were considered as mixed-phase samples and excluded from this series.

A typical XRD pattern is shown in Fig. 3. Besides the substrate peaks, indicated by asterisks, only the (00*l*) peaks of the *c*-axis 0212 phase are visible. The inset shows the low-angle part of the diffraction pattern with a series of diffraction peaks due to the finite size of the thin film. The observation of ''finite-size oscillations'' indicates that the film roughness is no greater than ± 1 unit cell.

In Fig. 4, the *c*-axis lattice parameter has been plotted against the Sr content of our films and of various bulk samples. Depending on the annealing conditions used, such as the magnitude of the O_2 pressure, the lattice parameters can be changed drastically. Here, values are reproduced for bulk samples annealed at 0.2 (▲ from Ref. 5 and ○ from Ref. 15), 1 (●), and 100 (▼) atm O_2.[5,14,15] As the oxygen

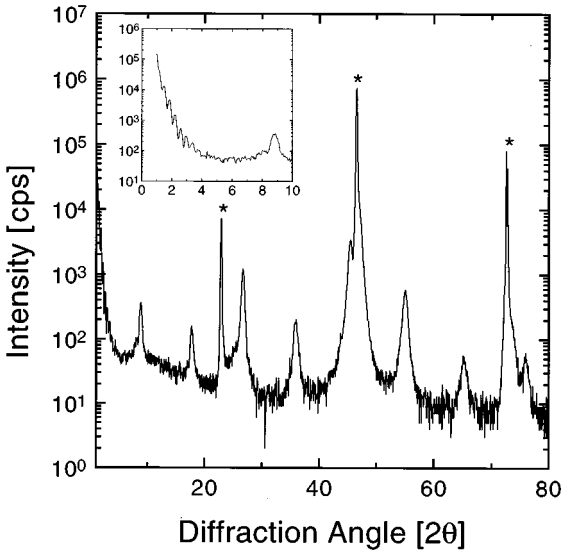

FIG. 3. X-ray-diffraction pattern of a c-axis 0212 thin film with a Sr content of 1.0 on an STO substrate. The peaks marked by asterisks are substrate peaks; the remainder are $00l_{0212}$ peaks. The inset shows a portion of the low-angle diffraction pattern indicating finite-size oscillations.

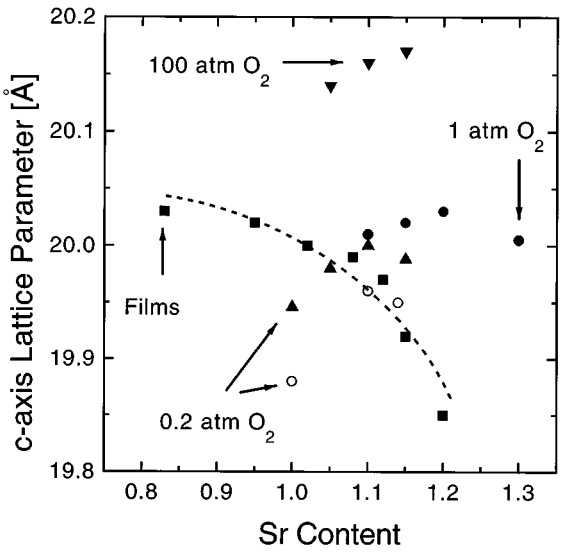

FIG. 4. c-axis lattice parameter of 0212 films as a function of Sr doping (■) the dashed line is a guide to the eye. Values obtained from bulk samples are also shown (●, ▲ ▼, ○).

pressure increases, more oxygen is incorporated in the lattice and the c-axis lattice parameter increases. Furthermore, for bulk samples, the strontium-content dependence of the c-axis lattice parameter displays a maximum. The position of this maximum gradually shifts towards higher Sr contents ($\simeq$ 1.1–1.2) as the oxygen pressure increases, while its curvature decreases. For the thin films, however, the maximum appears to be broader as well as being shifted to a considerably lower Sr content of $\simeq$ 0.8. The origin of these changes in the curves can be caused by one or a combination of several factors: the strontium content of the film, the oxygen content, residual epitaxial strain, or other microstructural phenomena, e.g., cation exchange. Let us consider each possibility in turn.

RBS data were obtained for the specimens of highest and lowest Sr contents showing the Sr content to be within 5% of the values expected; hence the Sr content is not at the origin of the changes in the curves. The shift of the maximum to lower Sr contents might correlate with a lower oxygen content (as for the bulk data), although it might be expected that the curve would also display a higher curvature and a much lower value for c at the maximum.

A film of composition $La_{2.17}Sr_{0.83}Cu_2O_{6+y}$ demonstrated low-resistivity as-grown (lower than that reported for bulk material) and a c-axis lattice parameter of 20.02 Å; after reduction under vacuum at 200 °C for 2 h, it had become insulating and the c-axis lattice parameter had decreased to 19.90 Å. ''Oxygen-rich 0212'' bulk material has been found to have a low resistivity, which increases with decreasing oxygen content. The behavior of both the c-axis lattice parameter and the resistivity indicates that the films do not suffer from a lack of oxygen. Furthermore, for films of $YBa_2Cu_3O_7$ (YBCO) and 214, the cooling procedure we use after film growth (under atomic oxygen) produces material with an oxygen content at least as high as for bulk material reacted under comparable oxygen activities.

A residual in-plane epitaxial tensile strain has previously been implicated for 214 on STO as playing a role in the reduction of the c-axis lattice parameter by about 0.04 Å (for a unit cell with c = 13.2 Å);[16,17] this in turn produces a small vertical displacement and a distortion of the c-axis versus Sr content curve instead of the large lateral ''shift'' observed in the 0212 case. A review of the critical role played by various types of defects and strain relaxation mechanisms in 214 thin films can be found in Ref. 18.

Because the Sr content, the oxygen content, and any residual epitaxial strain do not adequately explain the differences in the curves, there must be some other microstructural phenomenon. When the previous curve for the films is compared with that for the bulk material annealed at 1 atm O_2, it would appear that the crystal structure functions in a subtly different manner. One possible explanation is that the occupancy of the cation lattice sites is altered by the Sr ions. In the case of 214, substitution of Sr for La in the rocksalt layer, at constant oxygen content, leads to an increase of the c-axis lattice parameter, which tallies with the larger ionic radius of Sr.[19] Thus a reduction of the Sr occupancy of the rocksalt layer in the 0212 compound and, hence, an increase in the occupancy in the fluorite-type layers (these sites being of sufficient size to accommodate the larger cation) might be expected to reduce the c-axis parameter. This shift of the Sr ions to the fluorite sites may be promoted by a lower apparent oxygen pressure close to the conditions required to stabilize a CuO_2 plane configuration. In these circumstances a stable SrO-CuO-SrO stacking sequence could form first and subsequently be transformed to the ''infinite layer'' Sr-CuO_2-Sr sequence, the oxygen vacancies being in the fluorite-type layer. The same transformation applies for the bulk $SrCuO_2$ phase as pressure increases.[20] In this way the material behaves similarly to the Ca-doped 0212, in which the Ca preferentially occupies the fluorite-type layer, probably allowing the material to become superconducting.

2. Atomic force microscopy

The surface topography of the films was studied by means of an AFM. The image in Fig. 5 displays a scan area of 1.3

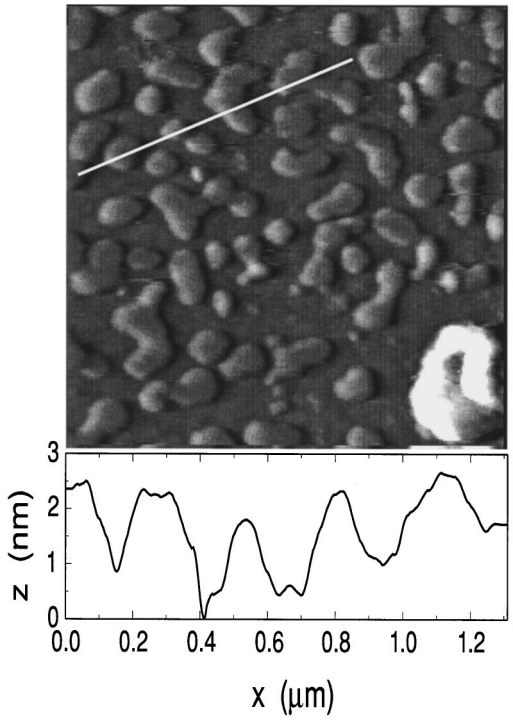

FIG. 5. A 1.3 μm $\times$ 1.3 μm AFM image and a horizontal profile of a *c*-axis 0212 thin film.

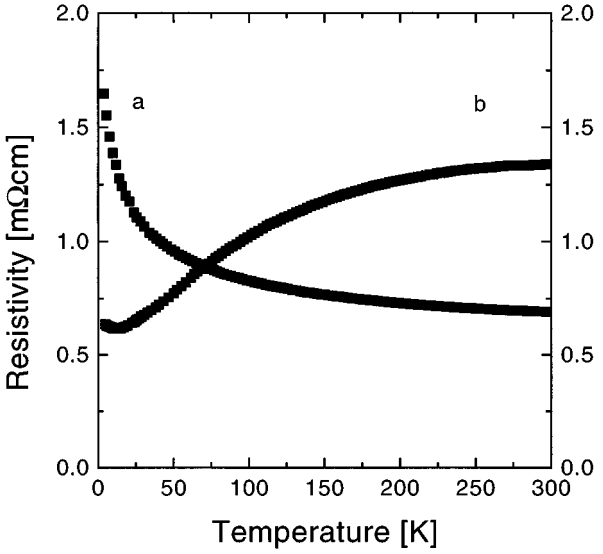

FIG. 6. Temperature dependence of the resistivity of a typical semiconducting [curve (a)] and a metallic [curve (b)] *c*-axis 0212 thin film.

μm $\times$ 1.3 μm with a *z* scale of 3 nm of the film with the largest Sr composition studied here ($La_{1.8}Sr_{1.2}Cu_2O_{6+y}$). Below the image a horizontal profile across the film surface is shown. Clearly visible in the lower right-hand corner is a typical CuO precipitate with a diameter of $\simeq$200–400 nm and a height of $\simeq$30 nm, as will be shown below using TEM. The remainder of the surface is predominantly two dimensional (2D) with large flat terraces, typically 200 nm wide, and steps of typically ± 1 unit cell (2 nm).

C. Normal-state properties

So far, it has not been possible to induce superconductivity in the pure Sr-doped 0212 compound, although the normal transport properties can be influenced significantly by either a change in Sr doping or annealing at different oxygen pressures. Unfortunately, however, little systematic data for the normal-state properties of the pure Sr-doped compound are available in the literature.[2] In Fig. 6, curve (a) shows the temperature-dependent resistivity for a sample with the composition $La_{1.8}Sr_{1.2}Cu_2O_{6+y}$. The observed semiconducting behavior is typical for most of these samples. However, the absolute values of the resistivity are lower than those obtained for the comparable bulk samples in the literature; this suggests a higher carrier density in the thin films. Therefore, it seems that the oxygen content of the films must be close to that of bulk samples, and that the above-mentioned values of the *c*-axis lattice parameters cannot be explained by a significant oxygen deficiency.

A totally different temperature dependence was found for the sample having the composition $La_{1.98}Sr_{1.02}Cu_2O_{6+y}$, curve (b) in Fig. 6, namely, *a metal-like resistivity* down to about 8 K; this, to our knowledge, has not previously been observed in this composition range. This particular film has a cation stoichiometry which in bulk materials would lead to an insulating behavior and has a *c*-axis lattice parameter of 20.00 Å, which is close to that of bulk samples. Therefore we speculate again that *the metal-like resistivity might be associated with a lattice site occupation different from that of the bulk compounds*.

In Fig. 7, the room-temperature resistivity of the series of films is shown. The two data points indicated by arrows correspond to films that have a thickness of 250 Å, whereas the others have a thickness of 400 Å; this difference is less relevant for the values of the lattice parameters, but thicker films have a slightly lower resistivity. As can be seen, de-

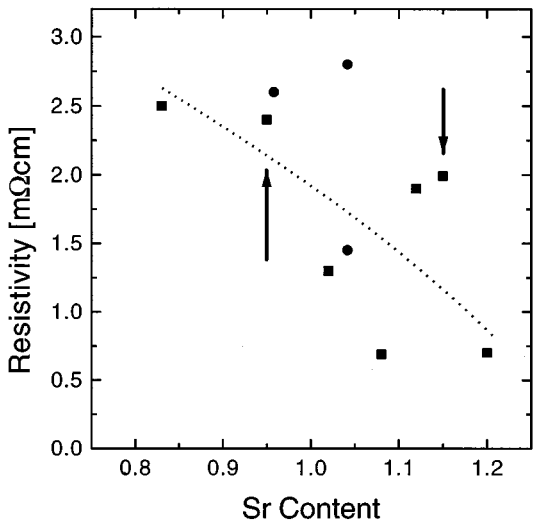

FIG. 7. Room-temperature resistivity of 0212 thin films (■) and of a few bulk samples (●) as a function of Sr content. The arrows indicate films with a thickness of 25 nm. The dotted line is a guide to the eye.

spite considerable scatter in the data, there is a trend towards improved conductivity with an increased Sr content. Besides the dependence on the Sr content, the value of the resistivity also depends critically on the oxygen content. As will be discussed below the actual amount of oxygen incorporated into the lattice is also determined by the microstructure and the availability of oxygen diffusion channels. At high Sr doping levels, several films have a low room-temperature resistivity, which is close to the value at which superconductivity generally appears in the high-T_c cuprates ($\simeq 1$ mΩ cm), *suggesting that it might be possible to induce superconductivity in some of these films*.

A thin-film-specific site occupation in the 0212 compound has not been reported so far. However, it is not unlikely that this exists as was demonstrated by the partial substitution and/or disordering of Ba by Y in $YBa_2Cu_3O_7$ thin films prepared under low-pressure conditions.[21–24]

D. Electrochemical oxidation

A feature which could explain the divergences between bulk and thin-film samples might be related to the microstructure of the films. In the case of 214 thin films, faults lying on the $\{111\}_{\text{ortho}}$ planes appear very often.[16] Their appearance and density depend mainly on the type of substrate but some variation is observed even among identical substrates. We have recently shown that these defects are excellent channels for oxidation both under electrochemical oxidation conditions[18,25,26] and during standard annealing procedures. The presence of these defects generally leads to well-oxidized thin films, but the variation in planar fault density from sample to sample can cause significant fluctuations.

As this material can be doped with oxygen by annealing under different oxygen pressures, we tried to insert oxygen using the electrochemical method developed recently for thin films.[25–27] To characterize the electrochemical activity of a film, an $I(E)$ cycle is performed; i.e., a voltage is applied between the sample (working electrode) and the reference electrode, while the current between the counterelectrode and the working electrode is measured. For a typical 214 thin film grown on STO, the voltammogram of an area ($S_g = 0.8$ cm^2) between 0.35 and 0.72 V exhibits three different regions [Fig. 8, curve (a)]. At low voltages (C_{I}, $E < 0.4$ V), the current rises linearly, which denotes the charging of the double layer at the interface between the electrolyte and the electrode. At intermediate voltages (O_{I}, $0.55 \leqslant E \leqslant 0.65$ V), the current saturates corresponding to a diffusion-limited reaction. This diffusion plateau has previously been ascribed[25–27] to an oxidation process of the 214 compound at the surface and in the planar faults according to the following general reaction:

$$La_2CuO_4 + 2\delta OH^- \rightleftharpoons La_2CuO_{4+\delta} + 2\delta e^- + \delta H_2O. \quad (1)$$

At the highest voltages of the curve (O_{II}, $E > 0.65$ V), the current increases again and the evolution of oxygen at the specimen surface takes place according to the reaction

$$4OH^- \rightleftharpoons O_2 + 2H_2O + 4e^-. \quad (2)$$

The oxidation (diffusion) plateau observed at $\simeq 550$ mV is only visible during the first $I(E)$ measurement — the oxygen diffusion from the surface and the planar faults into the bulk of the film is a slow process — and is proof that the material can be oxidized in this manner. In contrast, some 214 films grown on a $SrLaAlO_4$ (SLAO) substrate do not have these planar faults, their $I(E)$ curve shows no oxidation plateau, and they cannot be oxidized to the same extent as films on STO using the electrochemical oxidation method. However, this is not true for all 214 films on SLAO and it remains currently unknown which mechanism triggers the appearance or absence of these planar faults.

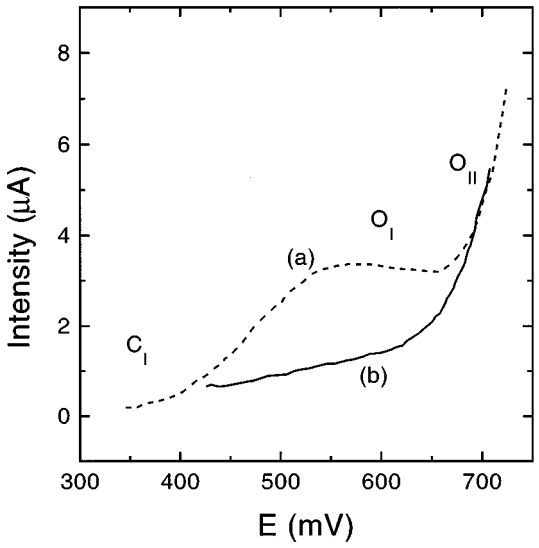

FIG. 8. $I(E)$ curves of (a) a c-axis 214 thin film and (b) a 0212 film, both grown on STO.

Figure 8 compares the first $I(E)$ curve of a 214 thin film (a) with that of a 0212 thin film (b). No oxidation plateau is observed for the latter film, suggesting that either this material cannot be oxidized electrochemically or that the appropriate defects such as planar faults are not present in a sufficiently high density. To our knowledge, such planar faults have not been reported for the 0212 compounds in the literature. This experiment was repeated for films with different Sr contents but the same results were obtained. As this compound can take up oxygen under a high-oxygen-pressure, high-temperature annealing treatment, we speculate that this is due to the lack of adequate diffusion channels required for electrochemical oxidation.

E. Microstructure

In the following, we provide a detailed microstructural analysis of one of these films, that with the highest Sr content in the series, i.e., $La_{1.8}Sr_{1.2}Cu_2O_{6+y}$.

1. Stacking sequence

Figure 9 gives a large-area cross section of the 40-nm-thick c-axis-oriented 0212 film grown on a $(001)SrTiO_3$ substrate. The epitaxial relationship between film and substrate as derived from XRD and TEM is the following: $[100]_{0212} \parallel [100]_{SrTiO_3}$, $[001]_{0212} \parallel [001]_{SrTiO_3}$.

The interface is atomically flat and contains no amorphous layer or second phase layer. There are ten possible

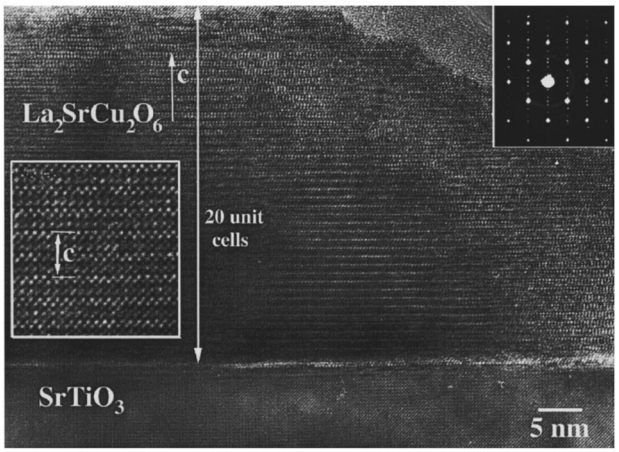

FIG. 9. Cross-sectional overview of the c-axis $La_2SrCu_2O_{6+y}$ thin film on $SrTiO_3$ with an enlarged view in the left-hand-side inset. The selected-area electron diffraction pattern in the right-hand-side inset confirms the c-axis orientation.

interface arrangements considering five inequivalent [001]-terminating planes in 0212 and two in $SrTiO_3$. Taking into account the work of Wen *et al.* [28] and our previous work on the interface YBCO/STO (Ref. 29) as well as other references[30–32] suggesting that the surface layer of $SrTiO_3$ is the TiO_2 layer, the possible interfacial structures are limited to 5. The substrate/thin-film interface was completely determined on the basis of HREM recordings. An example is given in Fig. 10 for a defocus value of -27 nm. The image averaged along the interface over a range of 15 nm is shown in inset (a). For this defocus value and thickness, the cation columns are imaged as black dots on a lighter background. The prominent, dotted white line in Fig. 10 is associated with the (La,Sr) layer with preferential La occupation and O vacancies (fluorite-type layer).

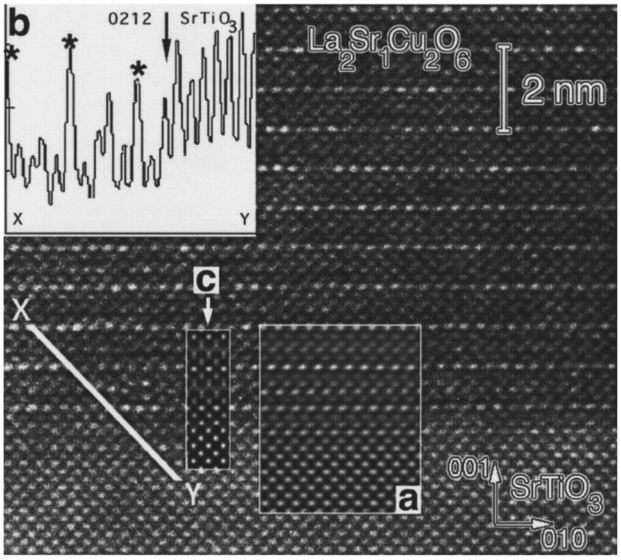

FIG. 10. HREM micrograph of the interfacial region at a defocus value of -27 nm with an image averaged along the interface direction in inset (a). Inset (b): line scan along the [011] direction indicated by the white line in the main image. Inset (c): simulation ($d=4$ nm, $\delta=-27$ nm) of the interface model 0212-(La,Sr)-CuO_2-(La,Sr)O-TiO_2-$SrTiO_3$.

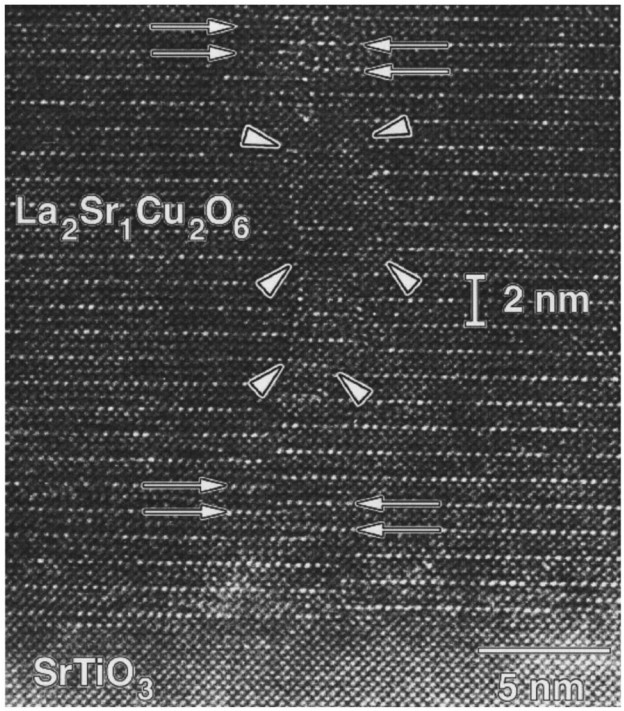

FIG. 11. [100]-HREM micrograph showing two types of stacking faults extending through the film.

Line intensity scans along the [001] axis or along $[\overline{0}11]$ allow us to determine the 0212 ending plane. The line scan along [011], indicated as a white line between X and Y in Fig. 10, is shown in inset (b) and indicates the second plane counting from the (La,Sr) planes, which are marked with an asterisk, i.e., (La,Sr)O as the ending plane on the basis of the difference in spacing between La-La and Sr-Ti. Image simulations of the five possible interface stackings were performed. The best fit to the image in Fig. 10 is found for a defocus of -27 nm and a thickness of 4 nm for the sequence 0212 – (La,Sr) - CuO_2 - (La,Sr)O - TiO_2 - $SrTiO_3$, of which the simulated image is shown as inset (c).

2. Out-of-phase boundaries

The structure of the film is generally very perfect, but out-of-phase boundaries roughly perpendicular to the film-substrate interface do occur regularly. The $[100]_p$ high-resolution micrograph in Fig. 11 shows such defects. In this example, the defects originate at a step in the $SrTiO_3$ substrate surface and extend throughout the entire film thickness with a defect plane $(hk0)$. Such planar defects may comprise two types of stacking faults, the respective shifts being highlighted either by arrows or arrowheads in Fig. 11. The out-of-phase boundaries or stacking faults, indicated by the arrows, have a displacement vector of $R=[00\frac{1}{5}]$. This displacement corresponds to the interplanar spacing between a (La,Sr) layer and the nearest (La,Sr)O layer; this is clear from the shift of the brighter lines in Fig. 11, which correspond to the (La,Sr) layer in the stacking sequence.

The stacking faults indicated by the arrowheads in Fig. 11 have a smaller displacement vector. In this case the displace-

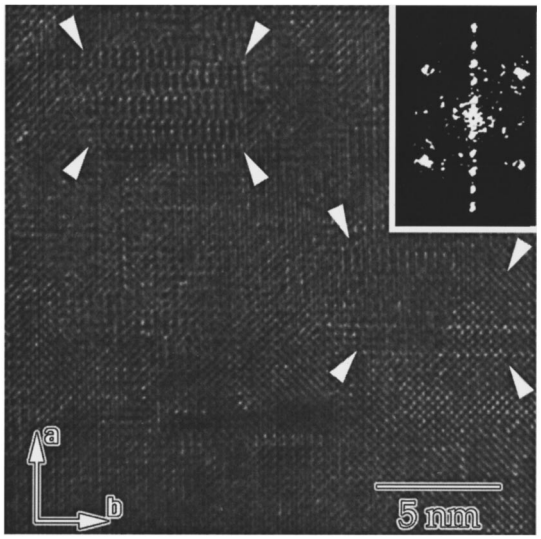

FIG. 12. [001]-HREM micrograph showing two 0212 *a*-axis grains, marked by arrowheads. The inset shows a computer diffractogram confirming the *a*-axis growth.

ment along [001] corresponds to a single layer shift from a (La,Sr) layer to a CuO_2 layer. This type of out-of-phase boundary occurs pairwise in a narrow region (4–5 nm), indicating that the displacement vector $R=[00\frac{1}{5}]$ is split into two components $R_1=[uv\frac{1}{10}]$ and $R_2=[-u-v\frac{1}{10}]$. Such extended defects, which originate at substrate surface steps, disconnect the CuO_2 layers responsible for high-T_c superconductivity and thus negatively influence the superconducting properties in that region.

Contrary to observations of 214 thin films on STO, these films do not show planar faults lying on the four {111} orthorhombic planes. As these faults are excellent oxygen diffusion channels,[26,33] their absence in 0212 films is a possible reason for the difficulty of electrochemically oxidizing the 0212 films.

3. Foreign phases and misoriented grains

AFM measurements (Fig. 5) of this film indicated that the surface of the 0212 films contains surface outgrowths of Cu-O. TEM combined with an energy-dispersive x-ray (EDX) analysis performed on the surface of the samples confirmed the identity of Cu-rich precipitates at the surface with a density of 2×10^7 cm^{-2} and an average diameter of 400 nm, in agreement with AFM measurements. The (220) planes of Cu_2O impurities produce a broad weak peak at 61.3° (0.15 nm) in the XRD spectrum (see also Fig. 3); the identification of this Cu-rich phase as Cu_2O is based on previous work regarding the origin of Cu-rich precipitates and the growth of CuO films.[34,35]

At the surface of the 0212 film very small (3 – 5 nm in diameter) ''precipitates'' occur (as seen in Fig. 12). The computer diffractogram, which is shown as an inset in Fig. 12, allows their identification as *a*-axis domains. Their *c* axis is oriented along a ⟨100⟩ axis of the surrounding 0212 structure. These 90° twin related domains do not nucleate from the substrate interface as *a*-axis regions, as is the case for YBCO (e.g., Ref. 36). They occur at the film surface and have a maximum thickness of 2 nm. They are purely a surface phenomenon of which no traces can be found deeper inside the film, possibly as a result of the film nucleation process. This possible explanation is related to the partial occupation of the oxygen sites in the fluorite layer. These sites in $La_2SrCu_2O_{6+y}$ are partially occupied, leaving anionic vacancies in the CuO_2 planes. This static disorder in $La_2SrCu_2O_{6+y}$ without correlation at long distances was interpreted by Caignaert *et al.*[7] to be an isolated defect with CuO_5 pyramids sharing corners along *c*. Such an isolated defect, in fact an incomplete unit cell in the *a*-axis-orientation, could act as the nucleus for an *a*-axis oriented grain. Indeed, under our deposition conditions, a phase with a lower Cu^{+II} content — such as the one associated with CuO_5 pyramids sharing corners — could be favored at the onset of nucleation of the phase. Such a nucleation process occurs not only at the beginning of the film growth on the substrate, but also during the deposition of the last block in every cycle of the block-by-block deposition process. Under the continuous bombardment of atomic oxygen, this phase is oxidized and subsequently reverts to the *c*-axis 0212 phase. Hence, one only expects this phase at the film surface.

4. $2\sqrt{2}a_p\times2\sqrt{2}a_p$ modulation

In plan-view sections of the $La_2SrCu_2O_{6+y}$ thin films, additional reflections appear locally, particularly in the [001]-zone diffraction pattern [Fig. 13(a)]. In addition to the strong basic spots at the perovskite positions (encircled) which belong to $La_2SrCu_2O_{6+y}$ and/or $SrTiO_3$, a mesh of weak but sharp spots can be observed. These additional spots can be indexed on the basis of a two-dimensional $2\sqrt{2}a_p\times2\sqrt{2}a_p$ superlattice cell. Tilting experiments around different axes, such as $[110]_p$ or $[100]_p$, reveal that the modulated structure has a c^* spacing (henceforth called

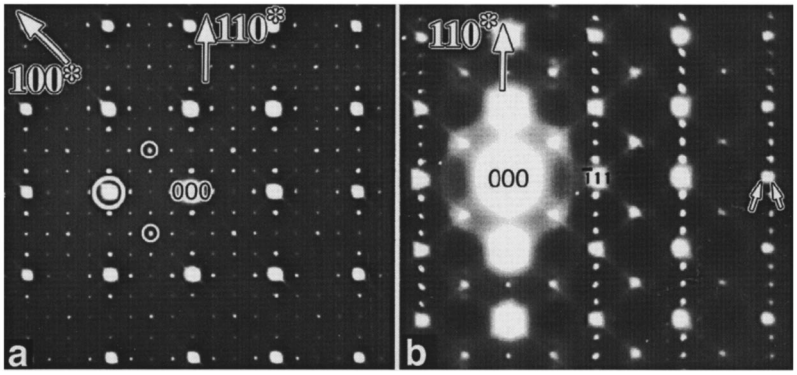

FIG. 13. (a) [001]-diffraction pattern of the film with the $2\sqrt{2}a_p\times2\sqrt{2}a_p$ superstructure. The basic perovskite reflections (encircled) are due to $La_2SrCu_2O_{6+y}$ and $SrTiO_3$. The weak but sharp reflections are due to the superstructure. (b) [112]-diffraction pattern, part of a tilting series around the $[110]_p$ axis. The rows of additional spots are shifted slightly with respect to the perovskite spots.

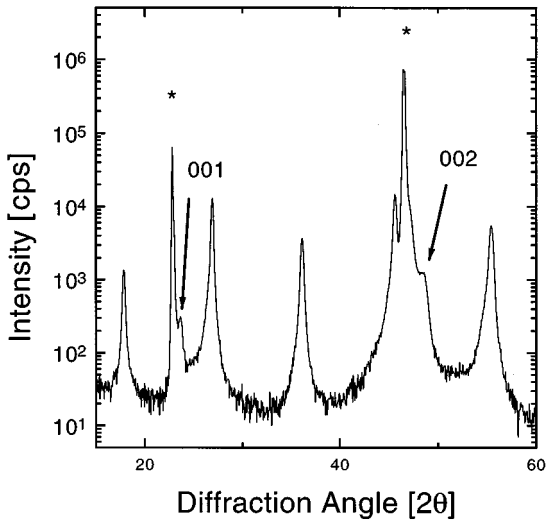

FIG. 14. X-ray-diffraction pattern of the c-axis 0212 thin film with a Sr content of 1.2 on an STO substrate. The peaks marked by an asterisk are substrate peaks. Besides the $(00l)$ peaks of the 0212 film, two peaks corresponding to the modulated superstructure are indicated.

c_s*) approximately equal to the perovskite spacing, i.e., certainly different from the short c* spacing of the 0212 reciprocal lattice.

The diffraction pattern of Fig. 13(b) shows the $[\overline{1}12]_p$ zone and reveals a misfit, indicated by arrows, of the superstructure reflections with respect to the perovskite spots of the substrate. From this misfit the c_s^* parameter of the $(2\sqrt{2}a_p\times 2\sqrt{2}a_p)$-modulated structure was calculated to be approximately 2.5% smaller than that of the $SrTiO_3$ substrate. This is confirmed by XRD (Fig. 14), where all peaks can be indexed as c-axis-oriented basic 0212 structures or as $SrTiO_3$ substrates, except for the lines corresponding to $d=0.376$ and 0.188 nm. These reflections can now be interpreted as the 001 and 002 reflections of the $2\sqrt{2}a_p\times 2\sqrt{2}a_p$ superstructure. The intensity of these reflections and the fact that the $2\sqrt{2}a_p\times 2\sqrt{2}a_p$ superstructure is only observed locally in plan-view sections allow an estimate of the amount of this phase in the sample, namely, $\simeq 5\%$.

A high-resolution micrograph of the $(2\sqrt{2}a_p\times 2\sqrt{2}a_p)$-modulated structure, taken along the $[001]_p$ zone, is presented in Fig. 15. This is a different area of the sample than the one used for the micrograph in Fig. 12. The modulation with a mesh of 1.1 nm along $[110]_p$ and $[110]_p$ directions is observed locally, superimposed on the pattern with a 0.39-nm spacing belonging to the basic lattice mesh indicated by white dots. The HREM image, however, does not allow conclusions to be drawn regarding the type of the modulation nor the plane(s) in which the modulation takes place.

In the literature on superconducting compounds several $(2\sqrt{2}a_p\times 2\sqrt{2}a_p)$-modulated structures have been reported; the first one being in $YBa_2Cu_3O_{7-d}$ (YBCO);[37,38] later a similar structure was reported in $Bi_{1.8}Pb_{0.4}Sr_2Ca_2Cu_3O_{10+x}$ (Bi-2212),[39] in high-pressure-synthesized $La_4Ca_4Cu_8O_{20+d}$,[40] and $La_4Ca_4Cu_8O_{18}$,[40] as well as in $La_{8-x}Sr_xCu_8O_{20}$ $(1.28<x<1.92)$.[11]

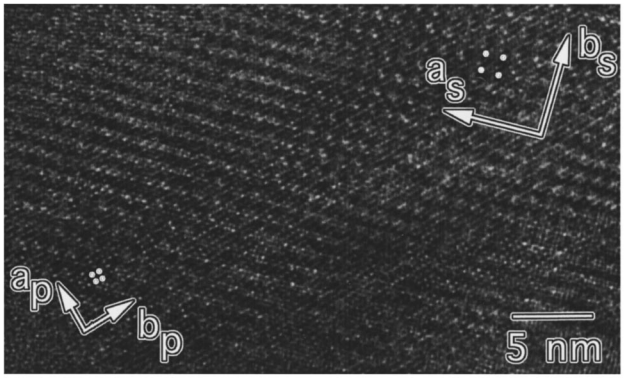

FIG. 15. [001]-HREM micrograph of an area of the thin film showing only the superlattices due to the $2\sqrt{2}a_p\times 2\sqrt{2}a_p$ modulation. The perovskite mesh is indicated by p.

In YBCO and in Bi-2212 the $2\sqrt{2}a_p\times 2\sqrt{2}a_p$ superstructure can be generated inside the electron microscope (*in situ*) at temperatures around 500 and 270 °C, respectively. The origin of this structure is still under debate, but careful TEM experiments allow the tetragonal superstructure to be attributed to a displacive modulation in the CuO_2 layers with a weak correlation between successive CuO_2 layers. However, in both YBCO and Bi-2212, the c axis of the modulated structure equals the c axis of the unmodulated YBCO or Bi-2212 structure.

In some La-based compounds the $2\sqrt{2}a_p\times 2\sqrt{2}a_p$ modulation of the basic perovskite structure appears as the room-temperature phase. The CuO_2 layers contain O vacancies and shifted Cu atoms. For instance the oxygen-deficient $La_{8-x}Sr_xCu_8O_{20}$ phase [i.e., $(La_{1-x}Sr_x)CuO_{2.5}$] has a tetragonal structure with lattice parameters $a=1.082$ nm, $c=0.386$ nm, and space group $P4/mbm$;[11] the stacking sequence in a unit slab is (La/Sr)O-$CuO_{1.5}$. The spacing between two $CuO_{1.5}$ planes in this structure is slightly larger (0.386 nm) than the spacing between the CuO_2 planes of the 0212 structure (0.366 nm).[7] Nevertheless, the modulation in the 808 modulated structure is closely related to that in the YBCO structure because the displacement pattern for the Cu atoms is similar in both structures.

One can only speculate about the formation mechanism or the exact structure of the local $2\sqrt{2}a_p\times 2\sqrt{2}a_p$ modulation in the 0212 structure. The $(La_{1-x}Sr_x)CuO_{2.5}$ structure is an oxygen-deficient layered perovskite structure which lacks one $(La_{1-x}Sr_x)O$ layer in the rocksalt-type lamella compared with the basic 0212 structure. In such a faulted structure a fraction of oxygen atoms would be displaced from the CuO_{2-x} planes towards the sandwiched La/Sr plane, resulting in a -$CuO_{1.5}$-(La/Sr)O-$CuO_{1.5}$- lamella which, when the accommodating displacements of the Cu and the remaining O atoms take place, becomes identical to the 808 structure, and thus can be responsible for the modulation. Hence for this modulation to appear, it seems important to replace the La/Sr fluorite-type layer by a La/Sr-O layer. It is known that a small fraction of excess oxygen is present at this site in the Sr-doped 0212 compound, contrary to the Ca-doped 0212 compound, owing to the preferential ninefold oxygen coordination of Sr compared to the eightfold oxygen coordination for Ca. This O transfer was reported for the

$La_2SrCu_2O_{6+y}$ structure in contrast to the $La_2CaCu_2O_{6+y}$ structure, as derived from neutron diffraction studies.[7,8] In addition, the very short *c*-axis lattice parameter reported above for these films suggests a much higher Sr occupation of the fluorite-type layer than what is found in bulk compounds, which would strongly favor the appearance of the $2\sqrt{2}a_p \times 2\sqrt{2}a_p$ modulation.

IV. CONCLUSION

Thin films of $La_{2\pm x}Sr_{1\mp x}Cu_2O_{6\pm y}$ were grown by MBE and characterized with emphasis on the normal transport and the structural (microstructural) properties. These properties are very different from those of bulk compounds with a similar composition, but they may be explained by a thin-film-specific site occupation of the La and Sr atoms in the lattice. Hence, these results demonstrate an interesting feature of MBE thin-film growth, i.e., the *possibility to obtain a different ionic site occupation of the various lattice sites from that of bulk materials*.

ACKNOWLEDGMENTS

The authors are grateful to L. Rossou, G. Stoffelen, and A. Vasiliev for TEM specimen preparation, and to P. Bauer for AFM measurements. K.V. acknowledges the Belgian national program on high-T_c superconductivity (Grant No. SU/03/17) and the IUAP-48 program for financial support; E.J.W. acknowledges the Swiss National Science Foundation NFP30 project for financial support.

*Present address: Essilor, Usine des Battants, F-55550 Ligny en Barrois, France.

[1] J. B. Torrance, Y. Tokura, A. I. Nazzal, and S. S. P. Parkin, Phys. Rev. Lett. **60**, 542 (1988).
[2] T. Tamegai and Y. Iye, Physica C **159**, 181 (1989).
[3] Y. Idemoto, M. Ohara, and K. Fueki, Physica C **229**, 361 (1994).
[4] R. J. Cava, B. Batlogg, R. B. van Dover, J. J. Krajewski, J. V. Waszczak, R. M. Fleming, W. F. Peck, Jr., P. Marsh, A. C. W. P. James, and L. F. Schneemeyer, Nature (London) **345**, 602 (1990).
[5] N. Nguyen, L. Er-Rakho, C. Michel, J. Choisnet, and B. Raveau, Mater. Res. Bull. **15**, 891 (1980).
[6] C. Michel and B. Raveau, Rev. Chim. Miner. **21**, 407 (1984).
[7] V. Caignaert, N. Nguyen, and B. Raveau, Mater. Res. Bull **25**, 199 (1990).
[8] P. Lightfoot, S. Pei, J. D. Jorgensen, X. -X. Tang, A. Manthiram, and J. B. Goodenough, Physica C **169**, 464 (1991).
[9] J. -P. Locquet and E. Mächler, J. Vac. Sci. Technol. A **10**, 3100 (1992).
[10] J. -P. Locquet and E. Mächler, MRS Bull. **19**, 39 (1994).
[11] L. Er-Rakho, C. Michel, and B. Raveau, J. Solid State Chem. **73**, 514 (1988); Y. Tokura, J. B. Torrance, A. Nazzal, T. C. Huang, and C. Oritz, J. Chem. Soc. **109**, 7555 (1987).
[12] H. Fujishita, M. Sera, and M. Sato, Physica C **175**, 165 (1991).
[13] J. Y. Lee, J. S. Kim, J. S. Swinnea, and H. Steinfink, J. Solid State **84**, 335 (1990).
[14] Y. Idemoto, M. Ohara, and K. Fueki, Physica C **229**, 361 (1994).
[15] F. Tresse (private communication).
[16] E. J. Williams, A. Cretton, Y. Jaccard, J.-P. Locquet, E. Mächler, P. Martinoli, and Ø. Fischer, in *Proceedings Microscopy & Microanalysis*, edited by G. W. Bailey, M. H. Ellisman, R. A. Henninger, and N. J. Zaluzec (Jones & Begell, New York, 1995), p. 382.
[17] J. -P. Locquet, Y. Jaccard, A. Cretton, E. J. Williams, F. Arrouy, E. Mächler, T. Schneider, Ø. Fischer, and P. Martinoli, Phys. Rev. B **54**, 7481 (1996).
[18] J. -P. Locquet and E. J. Williams, Acta Phys. Pol. A (to be published).
[19] J. -M. Tarascon, L. H. Greene, W. R. McKinnon, G. W. Hull, and T. H. Geballe, Science **235**, 1373 (1987).
[20] Z. Hiroi, M. Azuma, Y. Takeda, and M. Takano, in *Proceedings Sixth International Symposium on Superconductivity (ISS'93)*, Hiroshima, Japan, 1993, edited by T. Fujita and Y. Shishara (Springer, Tokyo, 1993), p. 285.
[21] J. L. MacManus-Driscoll, J. A. Alonso, P. C. Wang, T. H. Geballe, and J. C. Bravman, Physica C **232**, 288 (1994).
[22] V. Matijasevic, P. Rosenthal, K. Shinohara, A. F. Marshall, R. H. Hammond, and M. R. Beasley, J. Mater. Res. **6**, 682 (1991).
[23] J. Ye and K. Nakamura, Phys. Rev. B **50**, 7099 (1994).
[24] P. Schneider, G. Linker, R. Schneider, J. Reiner, and J. Geerk, Physica C (to be published).
[25] J. -P. Locquet, C. Gerber, A. Cretton, Y. Jaccard, E. J. Williams, and E. Mächler, Appl. Phys. A **57**, 211 (1993).
[26] F. Arrouy, J. -P. Locquet, E. J. Williams, E. Mächler, R. Berger, C. Gerber, C. Monroux, J. -C. Grenier, and A. Wattiaux, Phys. Rev. B **54**, 7512 (1996).
[27] J. C. Grenier, F. Arrouy, J.-P. Locquet, C. Monroux, M. Pouchard, A. Villesuzanne, and A. Wattiaux, in *Phase Separation in Cuprate Superconductors*, edited by E. Sigmund and K. A. Müller (Springer-Verlag, Berlin, 1994), p. 236.
[28] J. G. Wen, C. Traeholt, and H. W. Zandbergen, Physica C **205**, 354 (1993).
[29] A. Catana, J.-P. Locquet, and R. Broom, in *Proceedings ICAM 91*, edited by L. Correra (Elsevier, Amsterdam, 1992), p. 747.
[30] M. Kanai, T. Kawai, and S. Kawai, Jpn. J. Appl. Phys. 1 **31**, L331 (1992).
[31] H. Tanaka, T. Matsumoto, T. Kawai, and S. Kawai, Jpn. J. Appl. Phys. **32**, 1405 (1993).
[32] T. Hikito, T. Hanada, M. Kudo, and M. Kawai, J. Vac. Sci. Technol. A **11**, 2649 (1993).
[33] E. J. Williams, J. -P. Locquet, E. Mächler, Y. Jaccard, A. Cretton, R. F. Broom, C. Gerber, T. Schneider, P. Martinoli, and Ø. Fischer, Inst. Phys. Conf. Ser. **138**, 329 (1993).
[34] J. -P. Locquet, Y. Jaccard, C. Gerber, and E. Mächler, Appl. Phys. Lett. **63**, 1426 (1993).
[35] A. Catana, J. -P. Locquet, S. M. Paik, and I. K. Schuller, Phys. Rev. B **46**, 15 477 (1992).
[36] M. V. Sidorov and R. Oktyabrskii, Phys. Status Solidi A **126**, 427 (1991).
[37] M. A. Alario-Franco, C. Chaillout, J. J. Caponi, and J. Chenavas, Mater. Res. Bull. **22**, 1685 (1987).
[38] T. Krekels, T. S. Shi, J. Reyes-Gasga, G. Van Tendeloo, J. Van Landuyt, and S. Amelinckx, Physica C **167**, 677 (1990).
[39] T. Krekels, S. Kaesche, and G. Van Tendeloo, Physica C **248**, 317 (1995).
[40] A. M. Guloy, B. A. Scott, and R. A. Figat, J. Solid State Chem. **113**, 54 (1994).